# Identification of effective elastic modulus using modal analysis : application to canine cancellous bone

Margaux Blondel, Yara Abidine, Pauline Assemat, Sophie Palierne, Pascal Swider

# Identification of effective elastic modulus using modal analysis; application to canine cancellous bone

M. Blondel [a], Y. Abidine [b], P. Assemat [b], S. Palierne [a], P. Swider [b,*]

[a] National Veterinary School, Toulouse, France
[b] IMFT UMR 5502, Toulouse University, Toulouse, France

*Keywords:*
Bone mechanics
Cancellous bone
Modal analysis
Canine bone
Theoretical and experimental approach

A B S T R A C T

Mechanical properties of cancellous bone is of increasing interest due to its involvement in aging pathologies and oncology. Characterization of fragile bone tissue is challenging and available methodologies include quasi static compressive tests of small size specimens, ultrasound and indentation techniques. We hypothesized that modal analysis of flexure beams could be a complementary methodology to obtain Young modulus.

The sampling methodology was adapted such that the uniqueness of the linear dynamic response was available to determine the elastic modulus from natural frequencies and mode shapes. In a first step, the methodology was validated using a synthetic bone model as control. Then, water jet cutting allowed collecting fourteen small beam like specimens in canine distal femurs. X ray microtomography confirmed the microarchitecture preservation, the homogeneity and the isotropy at the specimen scale to derive effective properties. The first natural frequency in clamped free boundary conditions was used to obtain mean values of Young modulus, which ranged from 210 MPa to 280 MPa depending on the specimen collection site. Experimental tests were rapid and reproducible and our preliminary results were in good agreement with literature data. In conclusion, beam modal analysis could be considered for exploring mechanical properties of fragile and scarce biological tissues.

## 1. Introduction

The exploration of bone mechanical properties has focused on cortical bone, which is considered as the most mechanically competent tissue. However, characterization of cancellous bone is of increasing interest due to its involvement in aging pathologies and oncology (Morgan et al. 2018; Ordway et al. 2019). Cancellous bone mechanical properties are subjected to significant changes secondary to trauma, osteoporosis, neoplasia or therapeutic strategies such as minimally invasive osteosynthesis and chemotherapy (Greenwood et al., 2015; Goodheart et al. 2015).

Characterization of elastic properties of fragile bone tissue like cancellous bone is challenging. Main methodologies include quasi static compressive tests of small size specimens (Keaveny et al., 1997; Linde et al., 1991; Odgaard and Linde, 1991), ultrasound and indentation techniques (Linde et al., 1991; Rho, 1996; Dong et al., 2004; Prot et al., 2016; Vijayakumar and Quenneville, 2016; Daoui et al. 2017; Wu et al. 2018; Wear 2020). These techniques are complementary since they do not explore the tissue response at the same scale nor under identical physical stimulus. In those articles, the role of porosity, microarchitecture, anisotropy and boundary conditions on effective Young modulus have been examined and results showed a great sensitivity to samples in term of collection site, size, shapes, heterogeneity and anisotropy.

To address this characterisation challenge, modal analysis can be used to explore the dynamic behavior of structures and materials (Nashif et al.,1985; Ewins, 2000). This methodology has been applied in the literature to identify effective properties at the scale of the organ (Couteau et al. 1998; Neugebauer et al. 2011; Scholz et al., 2013; Henyš & Čapek,2017) or at tissue scale (Swider et al. 2009; Miyashita et al. 2018).

In case of complex dynamic responses and heterogeneous and anisotropic tissues, the problem is often under determined due to numerous unknown elastic coefficients in material laws. In this context, the challenge is to obtain the uniqueness of eigen values and eigen vectors pairs, i.e. natural frequencies and mode shapes. To untangle this problem, numerical methods such FEM associated with inverse numerical methods are often used (Swider et al. 1996; Taylor et al. 2002; Henyš & Čapek 2019) as theoretical solutions are rare. Experimentally, modal analysis benefits from non contact

* Corresponding author at: IMFT UMR 5502 CNRS – INPT – Toulouse 3, 2 allées C. Soula, 31400 Toulouse cedex, France.
*E-mail address:* pascal.swider@imft.fr (P. Swider).

measurement techniques and excitation force adaptation (Swider et al. 1994; Ewins 2000; Neugebauer et al. 2011).

In this article, we propose to adapt the sampling methodology such that the uniqueness of the theoretical dynamic response is available. Therefore, we hypothesize that beam modal analysis could be used to determine the effective elastic properties of bone tissue. This leads to sampling reduced size specimens accurate in geometry with homogeneous microstructure and isotropic behav ior. We used cancellous bone explanted from canine distal femurs as test tissue and the methodology was previously evaluated with polyurethane foam bone model.

## 2. Material and methods

In this section, the theoretical background is detailed before introducing the samples preparation method, the type of samples and the experimental method.

### 2.1. Governing equations of beam transverse motion

#### 2.1.1. Static response: Three points bending

The static three points bending test was used as a control test of the proposed methodology. Equation (1) gives the static elastic modulus $E_s$ as a function of the applied load $F$, the specimen length $l$, the section properties (width $b$, height $h$) and the mid span deflection $v(l/2)$ using the Timoshenko beam model (Timoshenko and Gere 1972). Shear effect is taken into account in the second term in brackets of equation (1). For a rectangular cross section and a span ($l/h$) greater than 10, shear coefficient $\alpha$ of 0.85 with $\nu$ lower than 0.5 gives a second order shear contribution.

$$E_s \quad \frac{Fl^3}{4bh^3}\frac{1}{v(l/2)}\left[1+\left(\frac{h}{l}\right)^2\frac{2(1+\upsilon)}{\alpha}\right] \tag{1}$$

#### 2.1.2. Theoretical modal analysis

The dynamic bending motion $v(x,t)$ of a uniform straight beam in its transversal plane is given by the governing equation (2) (Meirovitch, 1986; Lalanne et al. 1984) when secondary effects (shear, rotation inertia) and dissipative effects are negligible (Huang, 1961; Meirovitch 1986). Geometrical properties are the cross section $S$, the area moment of inertia $I$ and the beam span $l$. Effective material properties are the elastic modulus $E$ and the material density $\rho$.

$$EI\frac{\partial^4 v(x,t)}{\partial x^4}+\rho S\frac{\partial^2 v(x,t)}{\partial t^2} \quad 0 \tag{2}$$

The transverse motion $v(x,t)$ is written as the product of a space function or mode shape $\phi(x)$ by a time function $f(t)$ and equation (2) is transformed into equation (3a).

$$EI\frac{\partial^4\phi(x)}{\partial x^4}f(t)+\rho S\cdot\phi(x)\cdot\frac{\partial^2 f(t)}{\partial t^2} \quad 0 \tag{3a}$$

$$\text{with } v(x,t) \quad \phi(x)\cdot f(t) \tag{3b}$$

$$\text{and } \phi(x) \quad C\sin\beta x + D\cos\beta x + E\sinh\beta x + F\cosh\beta x \text{ with } C,D,E \text{ and } F \text{ constant.} \tag{3c}$$

Solutions of $f(t)$ are harmonic functions of angular frequency $\omega_n$ and the roots of the characteristic equation in space are expressed by equation (4a). Then, application of boundary conditions gives the transcendental equation, which is expressed by equation (4b) in case of clamped free conditions.

$$\beta_n \quad \sqrt[4]{\frac{\rho S\omega_n{}^2}{EI}} \; (a) \; 1+\cosh(\beta_n l)\cos(\beta_n l) \quad 0 \; (b) \tag{4}$$

The clamped free boundary conditions give the lowest frequen cies compared with other types of boundary conditions which is convenient with small, light and stiff specimens and the lowest root of equation (4b) was $\beta_1 = 1.875$. Using equation (4a), the effec tive modulus $E_d$ was expressed by equation (5a). The mode shape $\phi_1$ expressed by equation (5b) was determined using equation (3c) and (4a) together with boundary conditions that were $v(0) = \partial_x v(0) = 0$ at the clamped section and $\partial^2{}_x\, v(l) = \partial^3{}_x\, v(l) = 0$ at the free end.

$$E_d \quad \left(\frac{l}{1.875}\right)^4\frac{\rho S}{l}\omega_1{}^2 \text{ with } \omega_1(\text{rd/s}) \quad 2\pi f_1 \text{ and } f_1(Hz) \; : \; 1^{st}\text{resonance frequency} \tag{5a}$$

$$\phi_1 \quad \cosh\left(\frac{1.875}{l}x\right) \quad \cos\left(\frac{1.875}{l}x\right) \quad 0.734\left[\sinh\left(\frac{1.875}{l}x\right) \quad \sin\left(\frac{1.875}{l}x\right)\right] \tag{5b}$$

The response to forced harmonic excitation reaches maximal magnitude when the angular forcing frequency matches the angu lar frequency. Experimentally, natural frequency is found by using a swept sine or random noise in case of linear behaviour, and for low damping, amplitude resonance and phase resonance are iden tical (Nashif et al. 1985).

#### 2.1.3. Parameter sensitivity analysis

In the following, variables $p$ and $q$ successively correspond to parameters $l$, $b$, $h$, $\rho$, $\nu$ $F$ and $\omega$. Complete first order Taylor expan sion of relation (1) and (5a) gives uncertainty $\Delta E/E$ to specimen properties and measurement uncertainties. Details are given in appendix.

### 2.2. Specimen preparation

#### 2.2.1. Bone model specimen: Polyurethane foam

Sawbone® models #1522 02 representing a validated alterna tive for testing human cancellous bone were used as preliminary controls for static and dynamic tests (Thompson et al. 2003; Elfar et al. 2014). Four straight beams of 4 mm in width ($b$) and 40 mm in length were cut from a polyurethane sheet of 3 mm thickness ($h$) with an oscillating saw (IsoMet 1000, Buehler®) because sheet lightness was not adapted to the water jet machine used for canine femurs. For the three points bending test, the sam ple span was 30 mm. Manufacturer data were $E_s = 123$ MPa in com pression and $E_s = 173$ MPa in traction. The homogenous porosity was $\phi = 80\%$ and density was $\rho = 240$ kg/m$^3$.

#### 2.2.2. Canine cancellous bone specimen

Femurs were harvested from seven adult beagle dogs, which had died for reasons unrelated to orthopedic conditions. According to a validated protocol (Linde and Sørensen, 1993), bones were cleaned of soft tissues, wrapped in saline soaked gauze and stored frozen at 20 °C for less than 4 months.

The proximal extremity of each femur was embedded in polyur ethane resin (RenCast® FC 52/53 Isocyanate/FC 52 Polyol) as shown in Fig. 1a after having been thawed at room temperature and kept moist with saline soaked sponges (Brear et al., 1988). For embed ding, each femur was positioned so that a) the cranial and lateral anatomic axis were perpendicular to the mold bottom, b) the cau dal part of both femoral condyles was tangent to the back face of the mold and c) the lateral condyle slightly exceeded the lateral face of the mold. Orientations were controlled using two orthogo nal laser beam devices (PCL20; Bosch, Gerlingen, Germany).

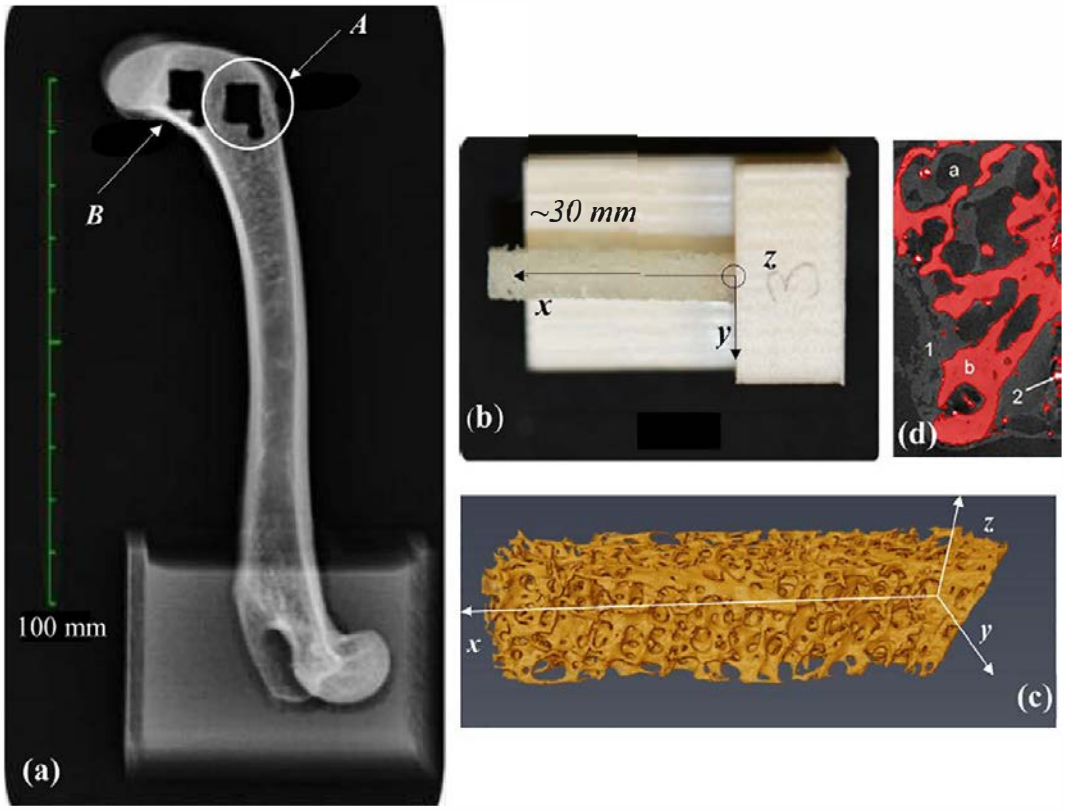


Fig. 1. (a) Medio-lateral X-ray image of the femur embedded into a polyurethane resin block after water cutting of specimen *A* (distal zone of the articular cartilage) and specimen *B* (proximal zone of the articular cartilage); (b) Cancellous bone specimen in clamped-free boundary conditions into the 3D-printed clamping fixture; (c) Microarchitecture of the specimen and (d) Partial view of a X-ray tomographic slice showing: pores - a, cancellous bone - b, clamping cyanoacrylate polymer –1 and abrasive particles –2 used in water-cutting process.

Embedded bones were stored at 20 °C and thawed at room temperature one day before specimen sampling.

Fourteen specimens were collected from the distal femoral epiphysis and metaphysis with a water jet cutting machine (WJA II; LDSA, Bar Le Duc, France) (Schwieger et al. 2004). Straight beams 4 to 5 mm in width ($b$) and 2 to 3 mm in height ($h$) were cut in the medio lateral direction. Seven specimens were classified in group *A*, and seven in group *B*, the latter being closer to the articular surface as shown in Fig. 1a. Any remaining cortical bone was removed with a scalpel blade. Geometrical properties were measured at three points on each specimen using a digital micrometer (LS 7000 series; Keyence SAS, Courbevoie, France) with an accuracy of 2 µm. The effective density was obtained by weighing (Metter Toledo®) each specimen with an accuracy of $10^{-6}$ kg, and by determining the specimen volume.

Fourteen samples were harvested from canine distal femurs; seven were classified in group *A*, and seven in group *B*.

### 2.3. Experimental methodology

#### 2.3.1. X ray micro tomography

Specimens were examined by X ray microtomography (Nanotom 180 Phoenix; GE Sensing, Labège, France) to explore the tissue microarchitecture. The scanner was operated at 80 kV and 90 µA with corrections for noise reduction and beam hardening to obtain images with voxel sizes of 10 × 10 × 10 µm. Images from six zones of *iso* length per specimen were explored using Avizo®(Thermo Fisher Scientific, Waltham, MA USA) and BoneJ (ImageJ ®) to determine porosity $\varphi$ and anisotropic degree *DA* (Harrigan & Mann 1984, Doube et al. 2010, Greenwood et al. 2015). No drying protocol was envisaged to preserve the limited number of available specimens, thus mass per unit length $\rho S$ used in equation (5a) was not accessible from micro CT.

#### 2.3.2. Static three point bending test

Three point bending tests were performed on bone model specimens (Sawbone®) using an electric testing machine (10 MH MTS; MTS Corporation®, Eden Prairie, MN USA) (Autefage et al., 2012). The beam span was 10 mm, the non destructive force applied at 0.1 mm/min was 10 N and data sampling was set to 10 Hz (Testwork® 4.08B, MTS). Using equation (1), three successive measurements of force and transverse displacements gave the mean effective Young modulus of each specimen.

#### 2.3.3. Experimental modal analysis

The specimen was clamped over 2 mm length in a 3D printed clamping fixture with cyanoacrylate polymer as shown in Fig. 1b, c and d. The free beam span was then measured with a depth gauge accurate to 20 µm. The specimen was clamped over 2 mm length in a 3D printed PLA fixture with cyanoacrylate polymer (CP) as shown in Fig. 1b, c and d. The fixture mass was 50 g whereas the specimen mass was 0.2 g. The Young modules of PLA and CP were 2.4 MPa and 1 GPa respectively. The significant changing of stiffness at the interface between the specimen and the fixture, associated with mass ratio reproduced the clamped conditions in term of strain and kinetic energies and matched the theoretical considerations developed in paragraph (2.1.2).

Specimens frequencies were obtained from the frequency response function (FRF), corresponding with the ratio of the beam transverse displacement $v(x,t)$ over the forced excitation $F(\Omega)$ in the frequency space (Ewins 2000). To generate the base excitation, the fixture was mounted on an electrodynamic shaker (K2007E01;

PCB® Piezotronics) using a piezoelectric force gauge (208C02; PCB® Piezotronics), (Fig. 2a and Fig. 2b). The transverse motion of the specimen was detected by using an optical displacement probe (CHRocodile unit 3 mm; Precitec®, spot diameter 12 μm, vertical resolution 40 nm), combined to a signal conditioner (CHRocodile 2S; Precitec®). A custom made 3 axis motorized system using translation actuator (Newport®) was used to map the specimen. Excitation, signal acquisition and post treatment were simultaneously controlled with a dynamic analyzer (OR34; Oros®). The base displacement was monitored imposing swept sine in the range 10 Hz 2 kHz and the linear behavior was verified by comparing responses with ascending and descending sweeps.

During vibration testing, cancellous bone specimens were sprayed with saline at room temperature (22 °C) to avoid dehydration. At least three FRF with the displacement probe pointed at three different locations along the beam span were performed on each specimen to obtain mean values and standard deviation of magnitude resonances and phase resonances, and to identify the mode shape $\phi_1$. Measurement time was less than one minute per specimen and no effect was detected on FRF.

## 3. – Results

### 3.1. Geometrical properties of specimens

Properties of polymeric foam beams (Sawbone®) used as control were: $b$ = 4.93 mm SD 0.1, $h$ = 3.42 mm SD 0.1 and $l$ = 40 mm SD 0.2. Measured density was $\rho$ = 248 kg/m$^3$ SD 16.

Geometry properties of fourteen biological specimens were $b$ = 4.82 mm SD 0.23 and $h$ = 2.6 mm SD 0.16. Straightness discrepancies corresponding with the mean value of relative standard deviation was 1.17% for $b$ and 1.77% for $h$ which approximately corresponded with 0.06 mm and 0.05 mm. Mass per unit length $\rho S$ used in equation (5a) was 1132 kg/m SD 90 and 1138 kg/m SD 110 for group A and group B, respectively.

For the experimental modal analysis, the mean free length of the specimens was $l$ = 18.94 mm SD = 3.3 mm. Specific geometrical properties ($l$, $b$, $h$) were used to determine the effective modulus $E_d$.

### 3.2. X ray microtomography of cancellous bone specimens

The porosity was determined for the six zones on each specimen using X ray tomography images post processing, each zone ranging from 2.4 mm to 3.3 mm in length. Porosity was homogenous with $\varphi$ = 0.775 SD 0.058 and degree of anisotropy (DA) tended to isotropic value (Doube et al. 2010) with $DA$ = 0.25 SD 0.05. Since $DA$ and fabric tensor are correlated (Zysset, 2003; Zbislaw 2012), isotropy at the beam scale was a validated assumption.

Detailed analysis of the acquisitions revealed two other types of materials. The first material corresponded to the cyanoacrylate polymer used to clamp the specimen, which saturated a few pores locally. The mean penetration length was 1.95 mm SD 0.34 and the reduction of free length was 10.6% SD 1.6. The second material represented the abrasive particles used during the cutting process (see Fig. 1.d). Their very low volume fraction, i.e. 0.54% SD 0.16, did not modify the mechanical response of the tissue.

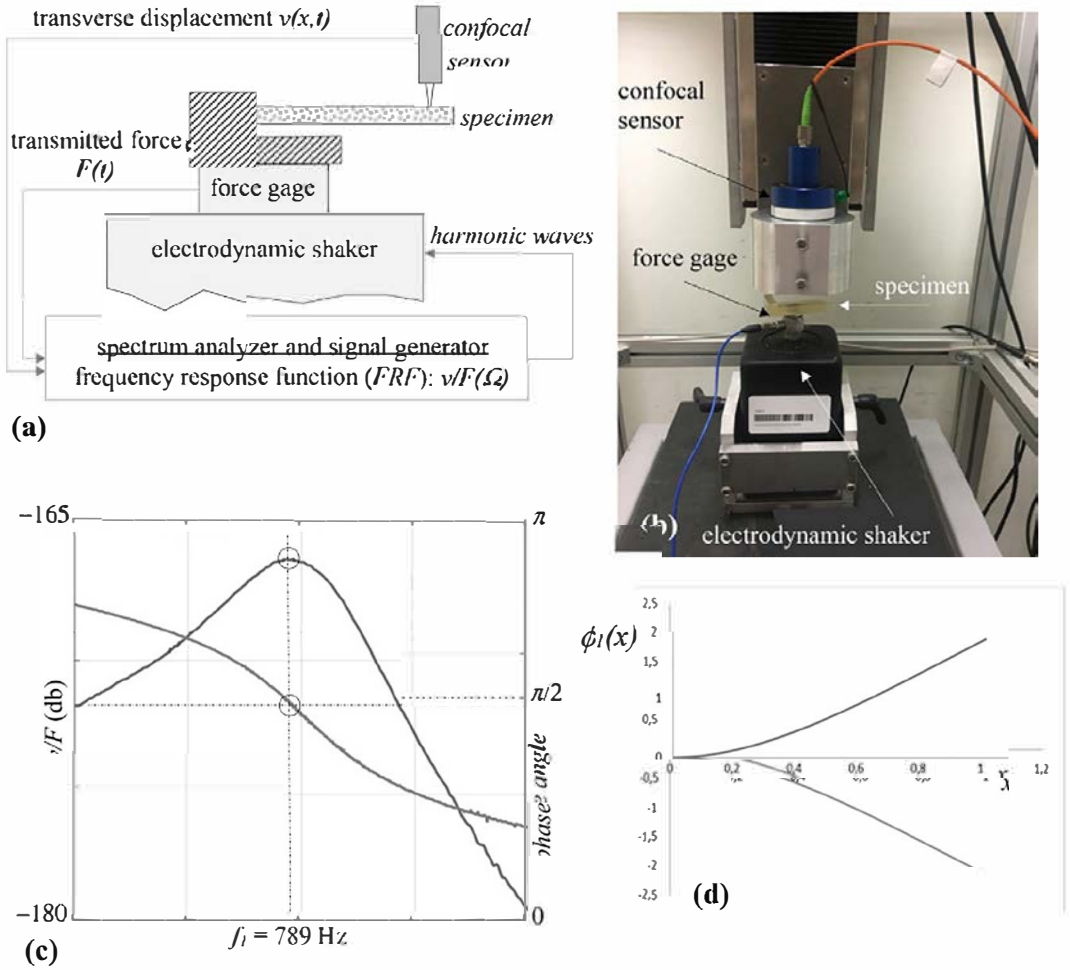


Fig. 2. (a) Diagram of the experimental dynamic device, (b) Experimental set-up, (c) FRF (magnitude and phase angle) of specimen #5 with $f_1$ = 789 Hz and (d) associated mode shape $\phi_1(x)$.

### 3.3. Comparison with control bone models (Sawbone®)

Results of the three point bending tests and of modal analysis are summarized in Table 1. The effective modulus obtained from equation (1) relative to bending tests was $E_s$ = 100 MPa SD 6 was correlated with manufacturer data ranging between 123 MPa and 173 MPa obtained with tensile tests.

Concerning the modal analysis, variations in frequency mea surements were less than 0.7% (repeatability test) and the effective modulus obtained from equation (7) was $E_d$ = 128 MPa SD20. This result was in good agreement with bending tests and manufacturer data.

### 3.4. Experimental modal analysis of canine cancellous bone specimens

Geometrical properties and frequencies of group *A* and group *B* are listed in Table 2 and Table 3, respectively. The natural frequen cies were obtained from at least three successive measurements of each specimen with ascending and descending swept sine and the relative standard deviation ranged from 0.1% to 2%. The FRF Bode diagram of specimen #5 in Fig. 2c shows a magnitude peak and a phases angle changing at $f_1$ = 789 Hz describing the first natural frequency. Phase resonance and magnitude resonance showed dis crepancies lower than 1%. The mode shape $\phi_1(x)$ described by equation (5b) was checked (Fig. 2d) by translating the confocal sensor along the specimen excited at the first resonance frequency. No other nodal points than the clamped zone and no signal cancel lation or dephasing was found and results were confirmed using portable strobe.

Effective modulus $E_d$ obtained from equation (7) were 211.5 MPa SD 18 and 279 MPa SD 52 for group *A* and group *B*, respectively. Group *B* showed significantly higher modulus, i.e. + 29%, with a $p$ value of 0.011 (Student test).

### 3.5. Parametric sensitivity analysis

Variation $\delta p$ corresponded with relative standard deviation of specimen properties measurement uncertainties calculated as variation ranges divided by mean values. In dynamics, the length sensitivity preceded those of height, frequency and density. Cross section width did not play any role. In statics, length and height showed similar influence before width, force and Poisson ratio. With $\delta p$ maximized to 2%, uncertainties were almost similar in static and dynamic for the effective Young modulus with $\Delta E/E$ equal to 14%. Direct terms of equation (A2) in appendix were prominent since cross terms were two orders lower.

## 4. Discussion and conclusion

We hypothesized that modal analysis of uniform straight beams in bending was a methodology adapted to the identification of effective elastic modulus (or Young modulus) of cancellous bone. Exact solutions of frequencies and mode shapes being available, difficulties due to complex structural geometry were circumvented to focus on material properties themselves. The relationship between eigen values eigen vectors and elastic properties had a unique solution. Water jet cutting allowed collecting beam like specimens in canine distal femurs with accuracy and agility while

**Table 1**
Effective Young modulus $E$ of control specimens (#1522–13 Sawbone®) in 3 points bending test (static) and experimental modal analysis. Control values* provided by the manufacturer were obtained with static compressive or traction tests.

| | Control value * | | Present study | |
|---|---|---|---|---|
| | compression | traction | 3 pts bending test | modal analysis |
| $E$ (MPa) | 123 | 173 | 100 SD 6 | 128 SD 20 |

**Table 2**
Geometrical properties, natural frequencies and effective Young modulus $E_d$ of specimens *A* collected from the zone more distal to the articular surface of the femoral epiphysis.

| specimen | $l$ ($10^{3}$m) | $b$ ($10^{3}$m) | $h$ ($10^{3}$m) | $\rho S$ ($10^{2}$ kg/m) | $f_1$ (Hz) | $E_d$ (MPa) |
|---|---|---|---|---|---|---|
| 1 | 13.8 | 4.9 | 2.83 | 1.435 | 1076.9 | 208.25 |
| 2 | 12.24 | 5.43 | 2.65 | 1.593 | 1284.4 | 222.67 |
| 3 | 15.33 | 4.97 | 2.51 | 1.388 | 805.0 | 241.25 |
| 4 | 15.66 | 4.81 | 2.74 | 1.562 | 759.9 | 210.95 |
| 5 | 14.53 | 4.67 | 2.54 | 1.438 | 789.0 | 199.82 |
| 6 | 11.23 | 4.65 | 2.64 | 1.547 | 1391.3 | 212.48 |
| 7 | 16.54 | 4.79 | 2.63 | 1.276 | 661.6 | 184.70 |
| | | | | mean $E_d$ = 210 MPa SD 19 | | |

**Table 3**
Geometrical properties, natural frequencies and effective Young modulus $E_d$ of specimens *B* collected from the zone more proximal to the articular surface of the femoral epiphysis.

| specimen | $l$ ($10^{3}$m) | $b$ ($10^{3}$m) | $h$ ($10^{3}$m) | $\rho S$ ($10^{2}$ kg/m) | $f_1$(Hz) | $E_d$ (MPa) |
|---|---|---|---|---|---|---|
| 9 | 17.65 | 4.47 | 2.4 | 1.418 | 590.1 | 298.71 |
| 10 | 16.78 | 4.86 | 2.55 | 1.505 | 755 | 324.84 |
| 11 | 21.93 | 5.1 | 2.16 | 1.310 | 337.5 | 257.47 |
| 12 | 15.42 | 4.93 | 2.81 | 1.554 | 771.25 | 182.61 |
| 13 | 22.15 | 4.88 | 2.7 | 1.439 | 475.62 | 314.17 |
| 14 | 19.85 | 4.71 | 2.63 | 1.252 | 534.42 | 248.18 |
| 15 | 20.98 | 4.60 | 2.61 | 1.225 | 541.63 | 326.59 |
| | | | | mean $E_d$ = 271.0 MPa SD 53 | | |

preserving tissue microarchitecture. Tissue integrity, homogeneity and isotropy were confirmed by X ray micro tomography to vali date the theoretical framework.

Base excitation on clamped free straight beam was well adapted to small, light and stiff structure. We used the first natural frequency of samples for which secondary effects of shear and rotation inertia had no relevant influence. The second frequency about six times higher was detected with some samples but the frequency dependence of elastic properties was not targeted.

The theoretical and experimental methodology has been vali dated with synthetic bone model used as control in statics and dynamics. Samples mimicking biological specimens were tested in static bending whereas data manufacturer were obtained from tensile tests. The local effects of boundary conditions and strain distribution patterns in cross sections could explain discrepancies. In return, modal analysis gave similar effective elastic modules since local effects were smoothed by the balance of modal strain energy and modal kinetic energy.

For tissue, modal analysis was prioritized to prevent alteration by static tests since few specimens were available. The shaping of biological samples allowed using the framework of transverse vibrations of flexure beams to get directly effective elastic modules from natural frequency measurement since mode shapes were pre dictable, unique and reproducible. Mean values of elastic modulus varying between 210 MPa and 280 MPa, were in agreement with uniaxial compressive tests ranging from 210 MPa and 315 MPa (Kang et al., 1998; Kuhn et al., 1989; Sumner et al., 1994; Vahey et al., 1987).

We proposed a preliminary application with a relative statisti cal power given the limited number of samples. Anyway, it seemed relevant enough to highlight property differences depending upon location and a significant increase of effective modulus when approaching the articular surface was found. This result, in agree ment with the literature (Vahey et al., 1987; Sumner et al., 1994), could be explained by a local mechanobiological remodelling due to increased strain energy which induced changes in tissue microarchitecture, porosity and stiffness.

The methodology for elastic modulus determination that we suggested was based on the exploration of one intrinsic property of a structure, which is its modal basis, i.e. mode shapes associated to natural frequencies (Lalanne et al., 1984; Meirovitch, 1986). The bending strain and stress fields into the beam like specimens were predominant, which allowed concluding that the effective elastic modulus (or Young modulus) was effectively the main actor of the structural response. For weakly dissipative structures, Lagran gian conservation smoothes the local influence of boundary condi tions in modal strain energy by the presence of the modal kinetic energy. Moreover, a resonance can be revealed with minimal input energy while being measured with great accuracy. The first order sensitivity analysis using maximum value of parameter uncertain ties concluded to a global uncertainty of tissue Young modulus lower than 14% which was a satisfactory result.

A limitation could concern the concept of effective elastic mod ulus underlying the proposed methodology. Indeed, cancellous bone was considered as a biphasic material, result of the minimal combination of a strongly porous medium drained by a fluid bone marrow. In static, it is possible to consider a negligible role of the fluid phase, which can be reasonably supposed, especially in com pressive tests, if fluid flow is drained at boundary conditions. In dynamic oscillations of low magnitudes, we can consider that the fluid phase acts mainly in mass but weakly contributes to the structure stiffness since the beam cross section is quasi constant during cycles. The mass effect is taken into account in the effective mass per unith length of samples.

In return, fluid structure interaction at the microscale may play a significant role in dissipative energy. These effects might modify the natural frequencies while shifting amplitude resonance from phase resonance. The derivation of elastic modulus can be updated with specific theoretical and experimental modal analysis of damped systems, if however this represents a significant impact compared to the uncertainties of measurement. This question can be addressed by implementing modal analysis of fresh tissue and dehydrated monophasic tissue. It could also help to interpret the differences between static and dynamic properties of biological tis sue. In addition, the second and third frequencies of beams are about six times and 17 times higher. Even if the second frequency was detected with some samples, it was generally more difficult to obtain them and exploring the frequency dependence of elastic properties was not the initial aim of the study.

In conclusion, beam modal analysis showed compelling aspects for the identification of mechanical cancellous bone properties. The methodology focused on Young modulus will be completed by Poisson ratio determination directly from torsion resonances. Inverse algorithms could also be implemented to simultaneously identify several elastic coefficients (Henyš and Čapek, 2017; Swider et al., 1996, 1998). In all cases the increased data base of biological specimen tested by modal analysis and static tests should confirm the methodology relevance.

The proposed methodology was rapid and reproducible, non destructive and adaptable to variable structure size. This could be reasonably exploited to characterize other fragile tissues, mate rials which elastic properties evolve rapidly in time, and small vol umes materials or tissues.

## Declaration of Competing Interest

The authors declare that they have no known competing finan cial interests or personal relationships that could have appeared to influence the work reported in this paper.

## Acknowledgements

The French Minister of Education and Research, the French National Center for research (CNRS) and the National Veterinary School of Toulouse (France) are acknowledged for their assistance. The study was partially funded by the Occitanie Region (France), grant RBIO 2015 INPT IMFT # 14054303.

## Appendix:

The first order Taylor expansion of function Young modulus $E$ at point $(p_0,q_0)$ is expressed by equation (A1), $\delta p$ and $\delta q$ being the small change in variables $p$ and $q$. In static, variables $p$ and $q$ repre sent specimen parameters and mechanical responses, i.e. force $F$ and displacement $v$ for static three point bending tests. In dynam ics, $p$ and $q$ represent specimen parameters and the natural fre quency $\omega_1$.

$$E(p_0+\delta p, q_0+\delta q) \quad E(p_0,q_0)+\delta p\partial_p E(p_0,q_0) + \delta q\partial_q E(p_0,q_0)+\delta p\delta q\partial^2_{p,q}E(p_0,q_0) + O\left(\delta^2 p,\delta^2 q\right) \tag{A-1}$$

Finally, the generic form of modulus uncertainty is expressed by equation (A 2).

$$\frac{\Delta E}{E} \quad \delta p\cdot\partial_p E/E+\delta q\cdot\partial_q E/E+\delta p\delta q\partial^2_{p,q}E/E+O\left(\delta_p^2,\delta_q^2\right) \tag{A-2}$$

with : $\partial_b E_d/E_d \quad 0; \partial_h E_d/E_d \quad \frac{2}{h}; \partial_l E_d/E_d \quad \frac{4}{l};$

$\partial_\rho E_d/E_d \quad \frac{1}{\rho}; \partial_\omega E_d/E_d \quad \frac{2}{\omega};$

$$\frac{\partial^2 E_d}{\partial h \partial l}/E_d \quad \frac{8}{hl}; \frac{\partial^2 E_d}{\partial h \partial \rho}/E_d \quad \frac{2}{\rho h}; \frac{\partial^2 E_d}{\partial h \partial \omega}/E_d \quad \frac{4}{h\omega};$$
$$\frac{\partial^2 E_d}{\partial l \partial \rho}/E_d \quad \frac{4}{l\rho}; \frac{\partial^2 E_d}{\partial l \partial \omega}/E_d \quad \frac{8}{l\omega}$$

$$\frac{\partial^2 E_d}{\partial \rho \partial \omega}/E_d \quad \frac{2}{\rho\omega}$$

and : $\partial_b E_s/E_s \quad \frac{1}{b}; \partial_h E_s/E_s \quad \frac{3}{h}; \partial_l E_s/E_s \quad \frac{3}{l};$
$\partial_F E_s/E_s \quad \frac{1}{F}; \partial_v E_s/E_s \quad \frac{1}{v};$

$$\frac{\partial^2 E_s}{\partial b \partial h}/E_s \quad \frac{3}{bh}; \frac{\partial^2 E_s}{\partial b \partial l}/E_s \quad \frac{3}{bl}; \frac{\partial^2 E_s}{\partial b \partial l}/E_s \quad \frac{3}{bl};$$
$$\frac{\partial^2 E_s}{\partial b \partial F}/E_s \quad \frac{1}{bF}; \frac{\partial^2 E_s}{\partial b \partial v}/E_s \quad \frac{1}{bv}; \frac{\partial^2 E_s}{\partial h \partial l}/E_s \quad \frac{9}{hl};$$

$$\frac{\partial^2 E_s}{\partial h \partial F}/E_s \quad \frac{3}{hF}; \frac{\partial^2 E_s}{\partial h \partial v}/E_s \quad \frac{3}{hv}; \frac{\partial^2 E_s}{\partial l \partial F}/E_s \quad \frac{3}{lF};$$
$$\frac{\partial^2 E_s}{\partial l \partial v}/E_s \quad \frac{3}{lv}; \frac{\partial^2 E_s}{\partial F \partial v}/E_s \quad \frac{1}{Fv}$$

## References


Autefage, A., Palierne, S., Charron, C., Swider, P., 2012. Effective mechanical properties of diaphyseal cortical bone in the canine femur. Vet J. 194, 202–209.

Brear, K., Currey, J.D., Raines, S., Smith, K.J., 1988. Density and temperature effects on some mechanical properties of cancellous bone. Eng. Med. 17, 163–167.

Couteau, B., Hobatho, M.C., Darmana, R., Brignola, J.C., Biomech, A.JYJ., 1998. Finite element modelling of the vibrational behaviour of the human femur using CT-based individualized geometrical and material properties. J. Biomechanics. 31 (4), 383–386.

Daoui, H., Cai, X., Boubenider, F., Laugier, P., Grimal, Q., 2017. Assessment of trabecular bone tissue elasticity with resonant ultrasound spectroscopy. J Mech Behav Biomed Mater. 74, 106–110.

Dong, X.N., Yeni, Y.N., Les, C.M., Fyhrie, D.P., 2004. Effects of end boundary conditions and specimen geometry on the viscoelastic properties of cancellous bone measured by dynamic mechanical analysis. J. Biomed. Mater. Res. A 68, 573–583.

Doube, M., Klosowski, M.M., Arganda-Carreras, I., Cordelières, F.P., Dougherty, R.P., Jackson, J.S., Schmid, B., Hutchinson, J.R., Shefelbine, S.J., 2010. BoneJ: free and extensible bone image analysis in ImageJ. 2010. Bone. 47 (6), 1076–1079.

Elfar, J., Menorca, R.M., Reed, J.D., Stanbury, S., 2014. Composite bone models in orthopaedic surgery research and education. J Am Acad Orthop Surg. 22 (2), 111–120.

Ewins, D.J., 2000. Modal Testing; theory, practice and application. Research studies press Ltd..

Goodheart, J.R., Cleary, R.J., Damron, T.A., Mann, K.A., 2015. Simulating activities of daily living with finite element analysis improves fracture prediction for patients with metastatic femoral lesions. J Orthop Res. 33 (8), 1226–1234.

Greenwood, C., Clement, J.G., Dicken, A.J., Evans, J.P.O., Lyburn, I.D., Martin, R.M., Rogers, K.D., Stone, N., Adams, G., Zioupos, P., 2015. The micro-architecture of human cancellous bone from fracture neck of femur patients in relation to the structural integrity and fracture toughness of the tissue. Bone Rep. 3, 67–75.

Harrigan, T.P., Mann, R.W., 1984. Characterization of microstructural anisotropy in orthotropic materials using a second rank tensor. J Mater Sci. 19, 761–767.

Henyš, P., Čapek, 2017. Material model of pelvic bone based on modal analysis: a studyon the composite bone. Biomech Model Mechanobiol. 16, 363–373.

Henyš, P., Čapek, 2019. Computational modal analysis of a composite pelvic bone: convergence and validation studies. Comp. Meth. Biomech. Biomed. Eng. 22, 916–924.

Huang, T.C., 1961. The effect of rotatory inertia and of shear deformation on the frequency and normal mode equations of uniform beams with simple end conditions. J. App. Mech. 28, 579–584.

Kang, Q., An, Y.H., Friedman, R.F., 1998. Mechanical properties and bone densities of canine trabecular bone. J. Mater. Sci. Mater. Med. 9, 263–267.

Keaveny, T.M., Pinilla, T.P., Crawford, R.P., Kopperdahl, D.L., Lou, A., 1997. Systematic and random errors in compression testing of trabecular bone. J. Orthop. Res. Off. Publ. Orthop. Res. Soc. 15, 101–110.

Kuhn, J.L., Goldstein, S.A., Ciarelli, M.J., Matthews, L.S., 1989. The limitations of canine trabecular bone as a model for human: a biomechanical study. J. Biomech. 22, 95–107.

Lalanne, M., Berthier, P., Der Hagopian, J., 1984. Mechanical Vibrations for. Wiley, USA.

Linde, F., Hvid, I., Madsen, F., 1991. The effect of specimen size and geometry on the mechanical behaviour of trabecular bone specimens. J. Biomech. 24, 454.

Linde, F., Sørensen, H.C., 1993. The effect of different storage methods on the mechanical properties of trabecular bone. J. Biomech. 26, 1249–1252.

Meirovitch, L., 1986. Elements of vibration analysis. McGraw-Hill, USA.

Miyashita, M., Ogawa, T., Naito, H., Shibamoto, A., Wang, A.S., Shobara, K., Sasaki, K., 2018. Evaluation of implant screw loosening by resonance frequency analysis with triaxial piezoelectric pick-up: in vitro model and in vivo animal study. Clin Oral Investig. 22 (5), 2129–2134.

Morgan, E.F., Unnikrisnan, G.U., Hussein, A.I., 2018. Bone mechanical properties in healthy and diseased states. Annu Rev Biomed Eng. 20, 119–143.

Nashif, A.D., Jones, D.I., Henderson, J.P., 1985. Vibration damping. John Wiley & Sons, New-York USA.

Neugebauer, R., Werner, M., Voigt, C., Steinke, H., Scholz, R., Scherer, S., Quickert, M., 2011. Experimental modal analysis on fresh-frozen human hemipelvic bones employing a 3D laser vibrometer for the purpose of modal parameter identification. J. Biomech. 44, 1610–1613.

Odgaard, A., Linde, F., 1991. The underestimation of Young's modulus in compressive testing of cancellous bone specimens. J. Biomech. 24, 691–698.

Ordway, N.R., Ash, K.J., Miller, M.A., Mann, K.A., Hayashi, K., 2019. A Biomechanical Comparison of Four Hip Arthroplasty Designs in a Canine Model. Vet Comp Orthop Traumatol. 32 (5), 369–375.

Prot, M., Cloete, T.J., Saletti, D., Laporte, S., 2016. The behavior of cancellous bone from quasi-static to dynamic strain rates with emphasis on the intermediate regime. J. Biomech. 49, 1050–1057.

Rho, J.Y., 1996. An ultrasonic method for measuring the elastic properties of human tibial cortical and cancellous bone. Ultrasonics 34 (8), 777–783.

Scholz, R., Hoffmann, F., von Sachsen, S., Drossel, W.-G., Klöhn, C., Voigt, C., 2013. Validation of density-elasticity relationships for finite element modeling of human pelvic bone by modal analysis. J. Biomech. 46, 2667–2673.

Schwieger, K., Carrero, V., Rentzsch, R., Becker, A., Bishop, N., Hille, E., Louis, H., Morlock, M., Honl, M., 2004. Abrasive water jet cutting as a new procedure for cutting cancellous bone–in vitro testing in comparison with the oscillating saw. J. Biomed. Mater. Res. B Appl. Biomater. 71, 223–228.

Sumner, D.R., Willke, T.L., Berzins, A., Turner, T.M., 1994. Distribution of Young's modulus in the cancellous bone of the proximal canine tibia. J. Biomech. 27, 1095–1099.

Swider, P., Ferraris, G., Vincent, B., 1994. Theoretical and experimental dynamic behavior of a golf club made of composite material. Modal Analysis : Int. J. Analytical and Experimental modal Analysis. 9, 57–69.

Swider, P., Le Fichoux, B., Jacquet-Richardet, G., 1996. Dynamic modelling of a composite plate, a mixed numerical and experimental approach. Composite Structures. 34)- 3, 301–308.

Swider, P., Jacquet-Richardet, G., Pereira, J.C., 1998. Interactions between numerical and experimental approaches in composite structure dynamics. Compos. Struct. 43, 127–135.

Swider, P., Guérin, G., Baas, J., Søballe, K., Bechtold, J.E., 2009. Characterization of bone-implant fixation using modal analysis: application to a press-fit implant model. J. Biomech. 42, 1643–1649.

Taylor, W.R., Roland, E., Ploeg, H., Hertig, D., Klabunde, R., Warner, M.D., Hobatho, M. C., Rakotomanana, L., Clift, S.E., 2002. Determination of orthotropic bone elastic constants using FEA and modal analysis. J. Biomech. 35, 767–773.

Timoshenko, S., Gere, J.M., 1972. Mechanics of Materials. Van Nostrand Reinhold Co..

Thompson, M.S., McCarthy, I.D., Lidgren, L., Ryd, L., 2003. Compressive and shear properties of commercially available polyurethane foams. J Biomech Eng. 125 (5), 732–734.

Vahey, J.W., Lewis, J.L., Vanderby, R., 1987. Elastic moduli, yield stress, and ultimate stress of cancellous bone in the canine proximal femur. J. Biomech. 20 (1), 29–33.

Vijayakumar, V., Quenneville, C.E., 2016. Quantifying the regional variations in the mechanical properties of cancellous bone of the tibia using indentation testing and quantitative computed tomographic imaging. Proc. Inst. Mech. Eng. [H] 230, 588–593.

Wu, D., Isaksson, P., Ferguson, S.J., Persson, C., 2018. Young's modulus of trabecular bone at the tissue level: A review. Acta Biomater. 15 (78), 1–12.

Wear, K.A., 2020. Mechanisms of Interaction of Ultrasound With Cancellous Bone: A Review. IEEE Trans Ultrason Ferroelectr Freq Control. 67 (3), 454–482.

Zbislaw, T., 2012. Equivalence of mean intercept length and gradient fabric tensors – 3d study. Med. Eng. Phys. 34 (5), 598–604.

Zysset, K., 2003. A review of morphology–elasticity relationships in human trabecular bone: theories and experiments. J. Biomech. 36 (10), 1469–1485.